Agricultural fertilization aggravates air pollution by stimulating soil nitrous acid emissions at high soil moisture

Yanan Wang[1†], Xiao Fu[1, ‡†], Dianming Wu[2], Mengdi Wang[2], Keding Lu[3], Yujing Mu[4, 5], Zhiguo Liu[4, 5], Yuanhang Zhang[3], Tao Wang[1]*

[1] Department of Civil and Environmental Engineering, The Hong Kong Polytechnic University, 999077 Hong Kong, China

[2] Key Laboratory of Geographic Information Sciences (Ministry of Education), School of Geographical Sciences, East China Normal University, 200241 Shanghai, China

[3] State Key Joint Laboratory of Environment Simulation and Pollution Control, College of Environmental Sciences and Engineering, Peking University, 100871 Beijing, China

[4] Research Center for Eco-Environmental Sciences, Chinese Academy of Sciences, 100085 Beijing, China

[5] University of Chinese Academy of Sciences, 100049 Beijing, China

‡ Now at Institute of Environment and Ecology, Tsinghua Shenzhen International Graduate School, Tsinghua University, 518055 Shenzhen, China

† These authors contributed equally to this work.

KEYWORDS: soil HONO emissions, fertilization, high soil moisture, model improvements, ambient air pollution.

ABSTRACT

Nitrogen lost from fertilized soil is a potentially large source of atmospheric nitrous acid (HONO), a major precursor of the hydroxyl radical. Yet, the impacts of fertilizer types and other influencing factors on HONO emissions are unknown. As a result, current state-of-the-art models lack an appropriate parameterization scheme to quantify the HONO impact on air quality after fertilization. Here, we report laboratory measurements of high HONO emissions from soils at 75%–95% water holding capacity after applying three common fertilizers, which contrasts to previous lower predictions at high soil moisture. Urea use leads to the largest release of HONO compared to the other two commonly used fertilizers (ammonium bicarbonate and ammonium nitrate). The significant promotion effect of fertilization lasted up to one week. Implementation of the lab-derived parametrization in a chemistry transport model (CMAQ) significantly improved post-fertilization HONO predictions at a rural site in the agriculture intensive North China Plain, and increased regionally averaged daytime OH,

O_3, and daily fine particulate nitrate concentrations by 41%, 8%, and 47%, respectively. The result of our study underscores the necessity to include this large post-fertilization HONO source in modeling air quality and atmospheric chemistry. Fertilizer structure adjustments may reduce HONO emissions and improve air quality in polluted regions with intense agriculture.

SYNOPSIS: Our research reveals large post-fertilization soil HONO emission and its significant impacts on air quality require worldwide attention.

INTRODUCTION

Nitrogen (N) fertilizer plays a key role in sustaining food production and the world population [1, 2]. The global N fertilizer consumption has increased from 11.3 Tg N yr^{-1} in 1961 to 109.1 Tg N yr^{-1} in 2017 [3, 4]. Due to low crop N use efficiency (<50% on average globally) [5, 6], a substantial fraction of surplus N is lost to the environment mainly through emissions and runoff, which causes adverse effects on water and air quality [7-10]. N loss from fertilized soils is a major source of reactive N species in the atmosphere. It has been long known that soils can emit nitric oxide (NO) and nitrous oxide (N_2O) resulting from soil microbial activities [11, 12], and later laboratory studies reveal that soils can also emit nitrous acid (HONO) with an emission flux comparable to that of NO [13, 14]. HONO is of great importance to atmospheric chemistry and air quality as photolysis of HONO is an important source of hydroxyl radical (OH) that regulates the atmospheric oxidation capacity and production of secondary pollutants

like ozone and some aerosols [15-18]. Yet, the sources of HONO, especially those in daytime, are not fully understood or quantified [19, 20].

HONO emitted from soil is produced through microbial processes of nitrification and denitrification [13, 14, 21]. The regulating factors of these processes are complex and diverse, and mainly include availability of soil N, organic matter content, soil moisture, pH, and temperature [22, 23]. Soil moisture affects HONO production via controlling the availability of oxygen (O_2) in soil that influences microbial activity [24]. Previous laboratory studies have shown that HONO fluxes from natural and agricultural soils typically peak at 0%–40% soil water holding capacity (WHC) and then decrease to a very low level at high soil water content (SWC) [13]. However, recent field measurements [25-28] observed a sharp increase in soil HONO emission immediately after fertilization when SWC is high as agricultural fertilization usually takes place along with rainfall or followed by irrigation [29]. This post-fertilization HONO source from soil has been suggested to be an important 'missing source' of ambient HONO in daytime [27, 30]. However, the effect of fertilizer types on HONO emission and its SWC dependence after fertilization are unknown, making it difficult to predict this HONO source and its atmospheric impact in air quality models.

In this study, we investigated the responses of HONO emissions from fertilized soil to SWC, fertilizer type, and the time since fertilization. We collected soil samples from croplands in northern and southern China and measured the soil HONO emission flux in a controlled dynamic chamber. We found that in addition to the promotion effect at

a low SWC, fertilizer applications can also greatly stimulate soil HONO emissions at a high SWC– a common condition for fertilized soil. Based on the laboratory results, we derived a parameterization scheme linking HONO emission to SWC for three commonly used fertilizers, and implement the scheme in a regional chemistry and transport model to quantify post-fertilization HONO emissions and its impact on ozone and nitrate aerosol in the North China Plain (NCP). We show that the soil HONO emissions significantly improved model HONO simulation and this source has important impact on regional air quality in the fertilization period.

MATERIALS AND METHODS

Soil samples. The soil samples used in this study were collected from two typical agricultural regions in China. S_{WD} was collected from a maize field (38.66° N, 115.25° E) in Wangdu County located in the NCP, which is one of the highest agricultural productivity regions in China [31], producing more than 50% and 33% of wheat and maize, respectively, in the country [32]. S_{HK} was collected from a vegetable field (22.43° N, 114.11° E) in Hong Kong, Southern China, which has a subtropical humid climate and produces of 10–15 vegetables and grains [33]. The soil properties and crop species in these two regions differ significantly and are representative of typical north–south differences in Chinese agriculture. At each site, five subsamples were collected from the top soil layer (5 cm) within 100 m^2 and were evenly mixed to minimize the influence of spatial variations of the soil properties [34]. The SWC of the field soil samples (SWC_{field}) was measured immediately after soil samples being shipped to the laboratory of the Hong

Kong Polytechnic University. All samples were then dried at room temperature, sieved to 2 mm to remove the gravel, roots, and litter and to homogenized the soil samples [35]. The soil samples were stored in a refrigerator at 4 °C until analysis.

HONO emission flux measurements. A Teflon dynamic chamber system (Figure S1) [13, 14, 21] was used to measure the HONO emission fluxes. 15.5 g of a prepared dry soil sample was placed in a glass petri dish (diameter = 50 mm) and wetted with ultrapure water (resistivity > 18 MΩ·cm) to its WHC value (equation (2)). The petri dish was then placed in the chamber to immediately measure the HONO emission flux [13, 14]. The air inlet was evenly distributed at the bottom of the chamber, and a small fan was placed inside the chamber to completely mix the gas. During incubation, the soil was dried under a constant stream of purified dry air with a flow rate of 6.3 L min^{-1}. A relative humidity (RH) sensor was applied to measure the RH at the chamber outlet, and the SWC was calculated by using the formula [13]:

$$SWC_{(t)} = 1 - \frac{\int_{t=0}^{t} RH(t)\cdot dt}{\int_{t=0}^{tmax} RH(t)\cdot dt} \frac{Mass_{water}}{Mass_{dry\ soil}} \cdot \frac{100}{WHC} \quad , \qquad (1)$$

where SWC(t) and RH(t) is the SWC and the relative humidity in the chamber, respectively, at time t. $Mass_{water}$ is the water mass (g) evaporated from the soil during experiment, $Mass_{dry\ soil}$ is the mass of dry soil(g), WHC is the ratio of the water mass in soil at saturation point to dry soil mass and is determined using filter method [36], given by:

$$WHC = \frac{Mass_{water(saturated)}}{Mass_{dry\ soil}}. \qquad (2)$$

The mixing ratio of HONO emitted from the soil samples was measured by a long path absorption photometer (LOPAP) (QUMA Elektronik & Analytik GmbH, Wuppertal, Germany) with a detection limit of 5 ppt. The entire sampling unit, including the chamber and LOPAP inlet, was operated in the dark and in a temperature-controlled cabinet to exclude photosensitized interferences. The emission fluxes were calculated as follows [13]:

$$F_N = \frac{Q}{A} \cdot [HONO]_{measured} \cdot \frac{M_N}{V_m} = \frac{Q}{A} \cdot (C_{out} - C_{in}) \cdot \frac{M_N}{V_m} \quad , \quad (3)$$

where F_N is the HONO emission flux in terms of N (ng N m^{-2} s^{-1}), Q is the chamber inlet flow rate (L s^{-1}), A is the petri dish area (m^2), $[HONO]_{measured}$ is the measured HONO mixing ratio (ppb), C_{out} and C_{in} are the mixing ratios of HONO (ppb) at the chamber outlet and inlet, respectively, and M_N (g mol^{-1}) and V_m (L mol^{-1}) are the molar mass of N and molar volume of the air, respectively.

We investigated the responses of HONO emissions to different N fertilizers by applying urea, NH_4HCO_3 and NH_4NO_3. For each fertilizer, we added 250 g of the soil sample to a glass beaker and calculated the water required by the soil samples to reach the target SWC_{field}. Next, a fertilizer equivalent to 100 kg N ha^{-1} (urea: 24.3 mg for S_{WD}, 19.7 mg for S_{HK}; NH_4HCO_3: 64.2 mg for S_{WD}, 51.9 mg for S_{HK}; NH_4NO_3: 32.5 mg for S_{WD}, 26.3 mg for S_{HK}) was dissolved in the water, added to the beaker and well mixed with the soil. The beaker was then covered by parafilm punctured with small holes to reduce the evaporation of water and ensure gas exchange between the beaker and air. During the experimental period after fertilization, 15.5 g of fertilized soil

139 subsamples were taken from the beaker at 8–24 hr intervals to measure the emission
140 fluxes following the step described above, until the emission flux reached the pre-
141 fertilization levels. These set of experiments aimed to determine the emission flux in
142 different days after fertilization. A total of 9, 6 and 5 subsamples were taken for S_{WD}
143 and 14, 11 and 10 subsamples for S_{HK} after urea, NH_4HCO_3 and NH_4NO_3 application,
144 respectively.

145 **Model Simulation.** The Community Multiscale Air Quality (CMAQ) model system
146 was applied to quantify the HONO emissions from fertilized soil and the impact on the
147 air quality. In the baseline simulation (Base), major HONO sources except soil
148 emissions, including vehicle emissions, gas-phase reactions of NO and OH, RH-
149 dependent and light-enhancing effects on heterogeneous reactions of NO_2, and the
150 photolysis of particle nitrate in the atmosphere and deposition on surfaces are
151 considered. And the detailed descriptions of these sources are given in a previous study
152 [18]. In the present study, we updated the rate constants of nitrate photolysis to take into
153 account of the effect of nitrate concentration on the rate constants, based on the works
154 of Ye et al [37, 38]. The detail reactions and parameters of these sources adopted in the
155 present study are listed in Table S1. The HONO uptake on the ground was incorporated
156 with an uptake coefficient of 1.0×10^{-5} [39].

157 The post-fertilization soil HONO emissions (F_N) are predicted as a function of soil
158 temperature (T) and soil water content (SWC), similar to the parameterization for soil
159 NO emissions[35, 40, 41]:

$$F_N = F_{N,max}(T_0, SWC_C) \cdot g(SWC_{fer}) \cdot h(T), \quad (4)$$

where $F_{N,max}$ is the maximum HONO flux at the optimum SWC (SWC_C) under a reference temperature T_0; $g(SWC_{fer})$ is the function of HONO emission as SWC; $h(T)$ is the temperature dependence of HONO emission and is expressed as ratio of HONO emission at T ($F_N(T)$) to that at T_0 ($F_N(T_0)$):

$$h(T)=\frac{F_N(T)}{F_N(T_0)}=\frac{A\cdot\exp\left[\left(\frac{-Ea}{R}\right)\cdot\frac{1}{T}\right]}{A\cdot\exp\left[\left(\frac{-Ea}{R}\right)\cdot\frac{1}{T_0}\right]}=\exp\left[\left(\frac{-Ea}{R}\right)\cdot\left(\frac{1}{T}-\frac{1}{T_0}\right)\right], \quad (5)$$

$F_N(T)$ takes the form of $A\cdot\exp\left[\left(\frac{-Ea}{R}\right)\cdot\frac{1}{T}\right]$, in which R is the gas constant (8.314 J mol^{-1} K^{-1}), Ea is the activation energy and is determined, together with constant A, by exponential fitting the HONO emission and temperature data obtained in our experiments (See Figure S4). $F_{N,max}(T_0, SWC_C) \cdot g(SWC_{fer})$ (See Results and Discussion section) and $h(T)$ are experimentally determined, and T_0 is 25 °C which is the room temperature under which the experiments are conducted.

To make use of the laboratory results to quantify the soil HONO emissions in the real ambient environment (F_{emis}), we used the following formula derived from a standard formalism that describes the atmosphere-soil exchange of trace gases [30, 42]:

$$F_{emis} = v_t \times [HONO]^* = v_t \times [HONO]_{measured} \quad , \quad (6)$$

where the transfer velocity (v_t) is from the CMAQ outputs, [HONO]* is the HONO equilibrium concentration at the soil surface [42], and $[HONO]_{measured}$ is the measured HONO mixing ratio at the chamber outlet. In our chamber system, the zero-air inlets were evenly distributed and a small fan was used to mix the air in the chamber (Figure S1). We assume that the air was well mixed in the chamber and [HONO]* was equal to

[HONO]$_{measured}$ (Figure S3). By combining equation (3-6), we can derive the soil HONO emissions in the real ambient environment (F_{emis}) as below:

$$F_{emis} = v_t \times [HONO]^* = v_t \times [HONO]_{measured} = v_t \times \frac{F_{N,max}(T_0, SWC_C) \cdot g(SWC_{fer})}{\frac{Q}{A} \cdot \frac{M_N}{V_m}} \times \exp\left[\left(\frac{-Ea}{R}\right) \cdot \left(\frac{1}{T} - \frac{1}{T_0}\right)\right] \quad , \quad (7)$$

The long-term observation data at 653 agriculture monitoring sites across China show that the SWC in most agricultural land is higher than 60% [43]. In view of the difficulty of accurately simulating soil moisture during fertilization that typically occurs along with irrigation, we incorporated the average, lowermost and uppermost soil HONO emissions in the SWC range of 60%–100% WHC after using urea (the dominant fertilizer in China) to represent the average case (SoilHONO_avg), lower limit case (SoilHONO_min) and upper limit case (SoilHONO_max).

The simulation domain covers land areas of China with a resolution of 36 km × 36 km based on a Lambert projection with two true latitudes of 25° N and 40° N, as illustrated in Figure 5a. The simulation period was 27–30 June 2014, and a previous four-day period was set as a spin-up time. The Weather Research and Forecasting Model (WRF) version 4.0 was applied to generate the meteorological field with the same physical options and inputs as described in Fu et al [44]. The minimum boundary layer height at night was set to 300m [45, 46], in view of underestimation by WRF in our study. The emission data were obtained from Zhao et al [47] for anthropogenic sources in 2015 and the Model of Emissions of Gases and Aerosols from Nature (MEGAN) [48] for biogenic emissions.

RESULTS AND DISCUSSION

HONO emissions from fertilized soils. We measured the HONO fluxes under different soil moisture for agricultural soil samples that were collected from Wangdu, Hebei province in Northern China (S_{WD}) and Hong Kong in Southern China (S_{HK}). Before fertilization, only one HONO emission peak was observed at a low SWC (the dry peak) in both soil samples. And the emission flux (F_N) was 341 ng m^{-2} s^{-1} at 41% WHC for S_{WD} (Figure 1a) and 78 ng m^{-2} s^{-1} at 18% WHC for S_{HK} (Figure 1b); it decreased to nearly zero at >60% WHC prior to fertilization for both samples. Similar phenomenon has been observed in previous study [13], and nitrification ($NH_4^+ \rightarrow NO_2^- \rightarrow NO_3^-$) is thought to predominate at low SWC, producing NO_2^- and then HONO (Figure 3). The small peak at high SWC (the wet peak) reported by Wu et al [14] did not occur or was too low to be observed in our soil samples.

We then separately applied three widely used N fertilizers, urea ($CO(NH_2)_2$), ammonium bicarbonate (NH_4HCO_3) and ammonium nitrate (NH_4NO_3) to the soil samples to investigate the response of soil HONO emissions to fertilization (see Methods). As shown in Figure 1c–1h, the dry peaks were significantly enhanced after fertilization and reached to a maximum 1–6 days later, with a maximum flux of 2100–3400 ng m^{-2} s^{-1} for S_{WD} and 5900–8300 ng m^{-2} s^{-1} for S_{HK} (Figure 2). The post-fertilization HONO emissions at low SWC increased by approximately 10 and 100 times for S_{WD} and S_{HK}, respectively. The elevated HONO emissions at low SWC is due to the increase of NH_4^+ amount in the nitrification process after fertilization. The

maximum dry peak occurred approximately 2 days later for urea use than NH_4HCO_3 and NH_4NO_3 for both samples, mainly because that urea is organic nitrogen and must be first hydrolyzed to NH_4^+-N by urease in soil within 2–3 days [49, 50].

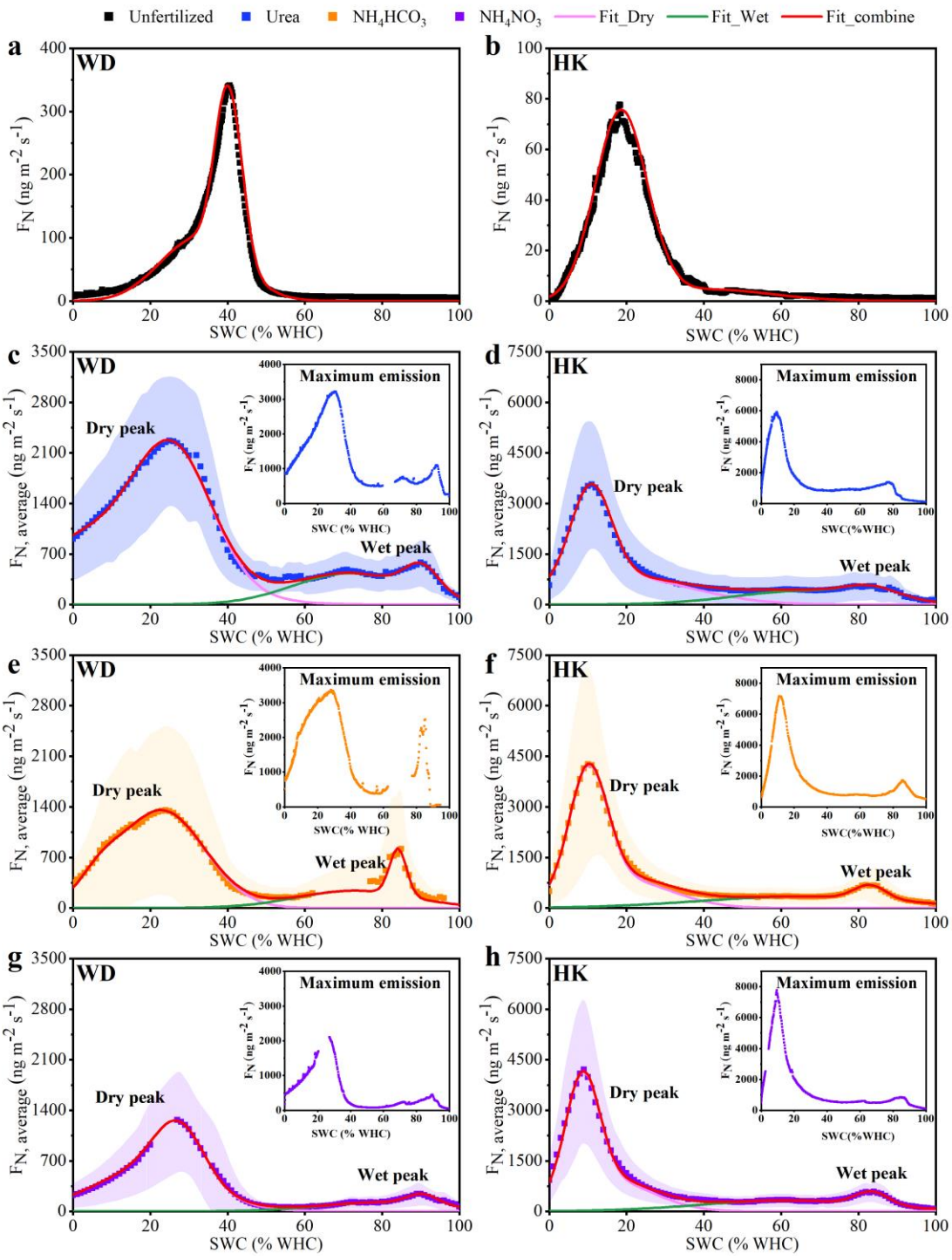

Figure 1. Soil emission fluxes of HONO as a function of the soil water content SWC (% water holding capacity, WHC). Soil HONO emissions before (a, b) and after applying urea (blue squares, c, d), NH_4HCO_3 (orange squares, e, f), and NH_4NO_3 (purple squares, g, h) to soil samples from Wangdu, Hebei province in Northern China (S_{WD}) and Hong Kong in Southern China (S_{HK}). The solid squares indicate the averaged emission results during the fertilization-affected period. The shadow areas represent the standard deviations. The pink, green and red lines represent the soil HONO emission fitting results at low SWC, high SWC, and the entire SWC range, respectively, as multiple Gaussian functions (Table 1). The upper right corner of c–h shows the maximum emission of the fertilized subsamples.

Differing from the extremely low pre-fertilization HONO emissions at high SWC, significant wet peaks are observed at >60% WHC for all of the fertilized soil subsamples from both sites and for different days (Figure 1c–1h), and they exhibit similar variations with time after fertilization to the dry peaks (Figure 2a, b). After the application of urea, NH_4HCO_3 and NH_4NO_3, the maximum wet peaks reached 1100, 2516 and 450 ng m^{-2} s^{-1} at 85%–93% WHC for S_{WD}, respectively, and 1460, 1725 and 1048 ng m^{-2} s^{-1} at 77–87% WHC for S_{HK}. These values were considerably higher than the pre-fertilization dry peaks. We took a weighted average of the HONO emission fluxes of each subsample against all of the fertilization-affected days and obtain averaged emissions ($F_{N,average}$) in Figure 1. The averaged emissions ($F_{N,average}$) of the wet peaks during the entire fertilization-affected period were 240–820 ng m^{-2} s^{-1}

(Figure 1c–1h). The boosted HONO emissions at high SWC may result from the addition of N fertilizer that provides substrate for microorganisms and increases the abundances of their functional genes [51-53], resulting in a wet peak of HONO emission via promoting both $NH_4^+ \rightarrow NO_2^-$ [12, 54-57] and $NO_3^- \rightarrow NO_2^-$ (Figure 3) [14] at high SWC (unsaturated) with limited oxygen content. The greater promoting effects of N fertilizer on HONO emissions for S_{HK} than for S_{WD} are possibly due to the different soil properties between the two samples. The pH values of S_{WD} and S_{HK} were 7.9 and 5.7, respectively. The alkaline condition (high pH) of S_{WD} is likely to lead more conversion of NH_4^+-N in three fertilizers to NH_3 followed by its volatilization loss [58, 59] and a low pH of S_{HK} favours HONO release from soil [30]. In addition to HONO, post-fertilization NO emissions also increased for both S_{WD} and S_{HK} at low SWC, while the effect of fertilization on NO emission at high SWC is not obvious (Figure S2). The average NO fluxes at 60%–100% WHC are only 1.7% and 1.0% of HONO fluxes in S_{WD} and S_{HK}, respectively.

The application of urea leads to the highest cumulative HONO emission for the whole fertilization-affected period, whereas NH_4NO_3 has the lowest emission, for both the dry and wet conditions (Figure 2c, d). For S_{WD}, the cumulative HONO emissions after urea application are 219% and 319% higher than NH_4NO_3 at low and high SWC, respectively; for S_{HK}, the cumulative promotion effects after using urea are 7% and 66% higher than NH_4NO_3 for dry and wet peaks, respectively. At low SWC, HONO is produced mainly by the nitrification process (Figure 3) and is boosted more by urea

than NH_4NO_3 due to more abundant reduced N in urea ($CO(NH_2)_2$) than NH_4NO_3 (2:1). At high SWC, soil HONO production is from both $NH_4^+ \rightarrow NO_2^-$ and $NO_3^- \rightarrow NO_2^-$. The higher HONO emission for urea than for NH_4NO_3 suggests that $NH_4^+ \rightarrow NO_2^-$ [12, 54-57, 60] is more important than $NO_3^- \rightarrow NO_2^-$ [14] because urea contains only reduced N. Additionally, urea can increase the content of soluble organic carbon [61], which is conducive to the growth of heterotrophic microorganisms and leads to increased production of NO_2^- [62]. The smaller difference between urea and NH_4NO_3 in S_{HK} suggest increased importance of the $NO_3^- \rightarrow NO_2^-$ process compared to S_{WD}.

The loss of soil N to HONO in the atmosphere after fertilization can be estimated as follows. We assume that the HONO emissions during the entire fertilization period reach the wet peaks as shown in Figure 2a and 2b, the proportion of cumulative HONO emitted (as N) during the entire fertilization period (Figure 2c, d) in the fertilizer usage in S_{WD} are 1.7%, 0.6%, and 0.3% for urea, NH_4HCO_3, and NH_4NO_3, respectively, and in S_{HK} are 5.4%, 1.5%, and 2.4% for urea, NH_4HCO_3, and NH_4NO_3, respectively.

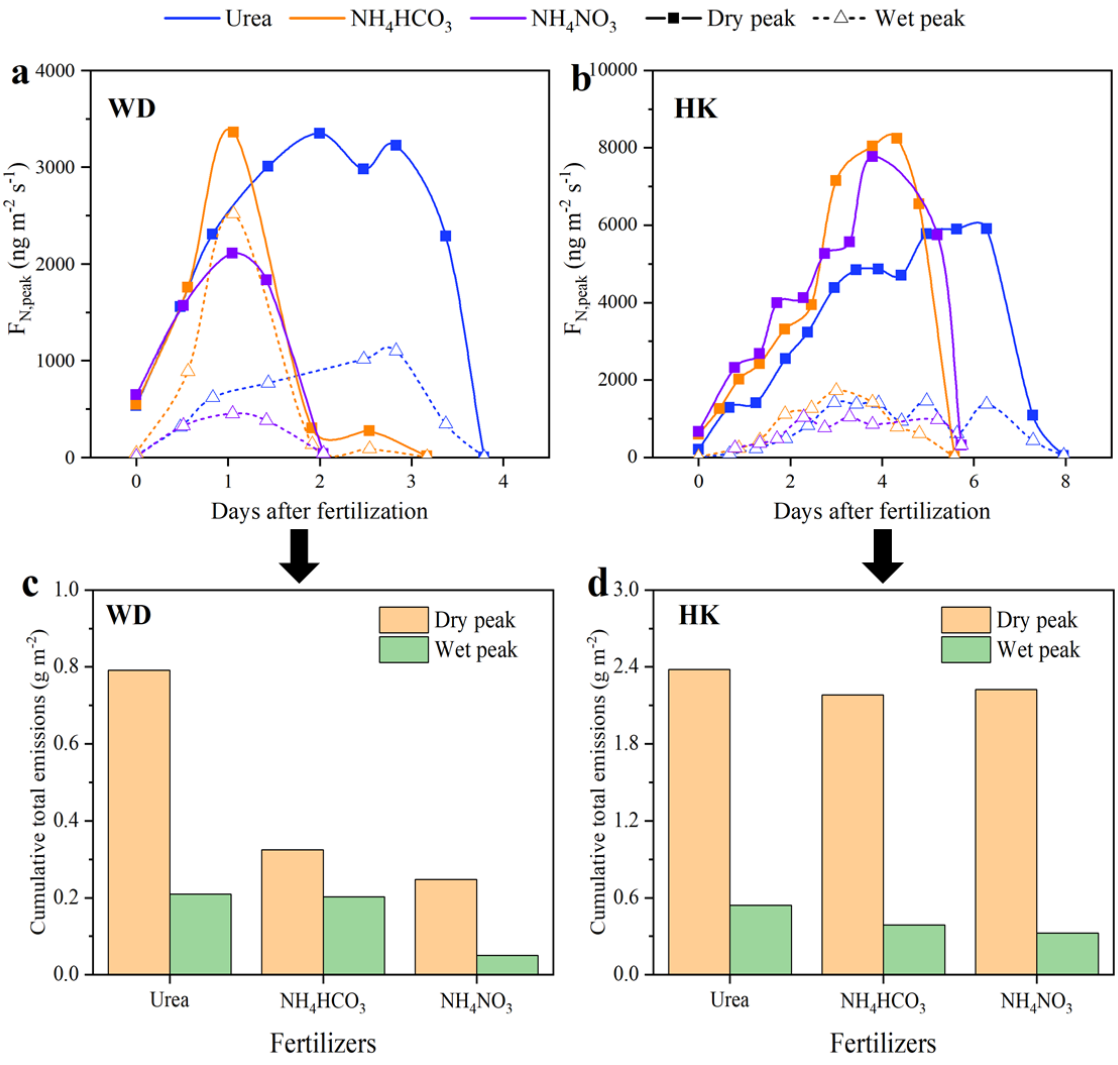

284

285 **Figure 2.** Variations of HONO emission peaks of subsamples and cumulative HONO
286 emissions during the fertilization-affected period. a and b show the variation of the peak
287 values as a function of days since fertilization for S_{WD} and S_{HK}, respectively (Dry peak:
288 solid square, Wet peak: open triangle; urea: blue, NH_4HCO_3: orange, and NH_4NO_3:
289 purple). c and d represent the integrated HONO emission after application of urea,
290 NH_4HCO_3, and NH_4NO_3 for S_{WD} and S_{HK}, respectively (Dry peak: yellow bars, wet
291 peak: green bars).

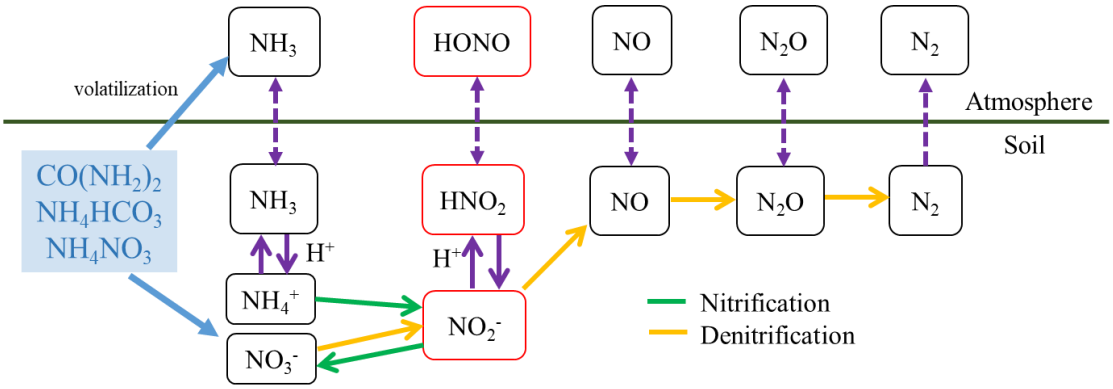

292

293 **Figure 3.** Key biological and physicochemical processes involved in soil HONO
294 emissions. Green and yellow arrows represent nitrification and denitrification processes,
295 respectively. Purple arrows represent physicochemical processes.

296 Based on the above experimental results, we derived a parameterization that links the
297 soil HONO emission flux at 25 °C (F_{N,T_0}) to SWC in equation (4) for air-quality model
298 use. Gaussian fitting was applied in Matlab 8.6 to fit the experimental data shown in
299 Figure 1 using the following formulation:

300 $$F_{N,T_0} = F_{N,max}(T_0, SWC_C) \cdot g(SWC_{fer}) = F_{N,max}(T_0, SWC_C)\exp\left(-\frac{(SWC-SWC_C)^2}{w^2}\right) \quad (8)$$

301 where SWC is the soil water content ranging from 0% to 100% WHC, SWC_C is the soil
302 water content at which the maximum HONO release rate ($F_{N,max}$) occurred, and w
303 characterizes the width of the fitting curves. As shown in Figure 1 and Figure S5, two
304 Gaussian functions well fit the dry peak (Dry1 + Dry2) in the low SWC range (0%–60%
305 WHC) and the wet peak (Wet1 + Wet2) in the high SWC range (60%–100% WHC),
306 respectively, for both S_{WD} and S_{HK}, in the form of:

$$F_{N(\text{Dry peak}),T_0} = F_{N,\max_{Dry1}} \cdot \exp\left(-\frac{\left(SWC-SWC_{C_{Dry1}}\right)^2}{w_{Dry1}{}^2}\right) + F_{N,\max_{Dry2}} \cdot \exp\left(-\frac{\left(SWC-SWC_{C_{Dry2}}\right)^2}{w_{Dry2}{}^2}\right), \quad (9)$$

$$F_{N(\text{Wet peak}),T_0} = F_{N,\max_{Wet1}} \cdot \exp\left(-\frac{\left(SWC-SWC_{C_{Wet1}}\right)^2}{w_{Wet1}{}^2}\right) + F_{N,\max_{Wet2}} \cdot \exp\left(-\frac{\left(SWC-SWC_{C_{Wet2}}\right)^2}{w_{Wet2}{}^2}\right). \quad (10)$$

Based on the input of F_N and SWC, the fitting procedure yielded $F_{N,max}$, SWC_c, and w which are listed in Table 1 for low and high SWC conditions of S_{WD} and S_{HK}. After combining with the formula for the temperature effect (Equation 7). The final formulation for the HONO emission (unit: ppb m s^{-1}) after applying N fertilizer of 100 kg N ha^{-1} at soil water content (SWC) and temperature (T) is shown below:

$$F_{emis} = F_{emis(\text{Dry peak})} + F_{emis(\text{Wet peak})} = v_t \times \frac{F_{N,max}(T_0,SWC_C)\cdot g(SWC_{fer})}{\frac{Q}{A}\cdot\frac{M_N}{V_m}} \times \exp\left[\left(\frac{-Ea}{R}\right)\cdot\left(\frac{1}{T}-\frac{1}{T_0}\right)\right] =$$

$$v_t \times \left[\frac{F_{N,\max_{Dry1}}\cdot\exp\left(-\frac{\left(SWC-SWC_{C_{Dry1}}\right)^2}{w_{Dry1}{}^2}\right)+F_{N,\max_{Dry2}}\cdot\exp\left(-\frac{\left(SWC-SWC_{C_{Dry2}}\right)^2}{w_{Dry2}{}^2}\right)}{\frac{6.3/60}{0.00196}\cdot\frac{14}{22.4}} + \frac{F_{N,\max_{Wet1}}\cdot\exp\left(-\frac{\left(SWC-SWC_{C_{Wet1}}\right)^2}{w_{Wet1}{}^2}\right)+F_{N,\max_{Wet2}}\cdot\exp\left(-\frac{\left(SWC-SWC_{C_{Wet2}}\right)^2}{w_{Wet2}{}^2}\right)}{\frac{6.3/60}{0.00196}\cdot\frac{14}{22.4}}\right] \times \exp\left[\left(\frac{-43990}{R}\right)\cdot\left(\frac{1}{T}-\frac{1}{298}\right)\right] \quad , \quad (11)$$

Table 1. Conceptual model of soil HONO emissions as multiple Gaussian functions of the soil water content (SWC). Dry1 and Dry2 represent the HONO emissions at low

323 SWC (0%–60% water holding capacity, WHC) and Wet1 and Wet2 represent the
324 HONO emissions at high SWC (60%–100% WHC).

Sites	Fertilizers	Parameters	Dry1	Dry2	Wet1	Wet2
WD	Unfertilized	$F_{N,max}$	99.00	265.90	--	--
		SWC_c	29.71	36.65	--	--
		w	13.03	4.04	--	--
	Urea	$F_{N,max}$	975.31	1623.84	433.53	377.29
		SWC_c	7.06	26.12	71.71	90.28
		w	28.81	13.90	20.74	6.43
	NH_4HCO_3	$F_{N,max}$	284.29	1357.77	240.05	645.91
		SWC_c	6.84	22.91	72.83	84.11
		w	7.53	15.63	21.29	3.09
	NH_4NO_3	$F_{N,max}$	572.21	766.40	125.16	142.87
		SWC_c	19.21	27.38	79.92	90.43
		w	20.16	9.08	22.75	5.61
HK	Unfertilized	$F_{N,max}$	74.24	4.51	--	--
		SWC_c	18.55	42.02	--	--
		w	9.48	21.99	--	--
	Urea	$F_{N,max}$	2837.35	819.90	403.16	322.76
		SWC_c	10.79	18.39	65.66	83.45
		w	7.43	25.51	25.18	9.93
	NH_4HCO_3	$F_{N,max}$	3594.82	830.73	340.66	419.88
		SWC_c	10.09	18.88	64.81	83.00
		w	6.91	17.78	36.96	5.86
	NH_4NO_3	$F_{N,max}$	3388.2	908.04	324.72	390.58
		SWC_c	8.59	15.39	61.58	83.51
		w	6.19	16.08	32.03	6.12

Simulations of post-fertilization HONO emissions and its impact on air quality. We next implement the HONO emission scheme in the CMAQ model (see Methods) and simulate the HONO during a typical fertilization event in the NCP. High ambient HONO levels were observed following fertilization during 27-30 June 2014 at an agricultural site in Wangdu [27], with the peak HONO mixing ratio of ~2.4 ppb at nighttime and ~0.9 ppb at noon (Figure 4b). As the information on the fertilizer use for this fertilization event was not available, we adopted our lab measured HONO emission for 100 kg N ha^{-1} which is a typical fertilization use in the NCP [63]. Soil fertilization by individual farmers in a large agricultural region like NCP can take place at the different time, and the impact of fertilization on the atmosphere is influenced by the average effect of these fertilization activities. In order to obtain the average effect of fertilization on HONO emissions, we used averaged emissions ($F_{N,average}$) shown in Figure 1 in the model simulations. As the NO emission does not show significant increase at high SWC after fertilization (Figure S2), we did not include soil NO emission in our model simulations.

Figure S6 shows the comparison of simulated and observed temperature, relative humidity and wind speed at Wangdu site, with the normalized mean bias (NMB) of -2.1%, -9.8% and 28.2%. The results indicate the Weather Research & Forecasting Model (WRF) used in this study reasonably reproduced these key surface meteorological parameters. As shown in Figure 4b, the model simulation without soil

346 emissions (Base) underestimates the ambient HONO levels by −54%, −76% and −45%
347 for the daily, daytime (6:00–18:00) and nighttime averages, respectively, despite the
348 fact that model has included most other known sources (e.g., heterogeneous reactions
349 of NO_2 on the ground and aerosol surface, photolysis of nitrate, etc., see Methods).
350 With the implementation of the soil emission assuming a uniform use of urea fertilizer
351 of 100 kg N ha^{-1} in the model domain, the modelled soil HONO emissions (F_{emis}) show
352 a pronounced diurnal variation (Figure 4a), with higher emissions in daytime than
353 nighttime due to the impacts of the increasing transfer velocity and soil temperature in
354 daytime. The daytime peak values vary in the range of 20–196 ng N m^2 s^{-1} with an
355 average of ~80 ng N m^2 s^{-1}. The lowest values at nighttime are in the range of 0.1–9 ng
356 N m^2 s^{-1}, with an average of ~4 ng N m^2 s^{-1}. The diurnal pattern and magnitude of the
357 soil HONO emissions are consistent with previous field observed HONO flux with
358 open-top chambers at Wangdu site [25, 26]. The inclusion of soil HONO emissions at high
359 SWC improved the model performance for ambient HONO simulations at Wangdu for
360 the study case. The observed values at night are generally in the range between the
361 lower and upper simulated limits due to variation in the soil water content. The
362 simulated nighttime average HONO levels by SoilHONO_avg increased from 0.8 ppb
363 to 1.8 ppb, with the NMB decreasing from −45% to 33% (Figure 4b). The daytime
364 HONO simulation was also improved, with the NMB decreasing from −76% to −29%.
365 However, underestimation of HONO at noontime remains considerable, possibly due
366 to the contributions of missing photosensitive sources and the difficulty in simulating

local emissions and meteorology with a regional model. Figure S7 shows the comparison of simulated and observed NO_2 concentrations at Wangdu site. The simulation can generally catch the hourly variations. The inclusion of soil HONO emissions (SoilHONO_avg) increased the simulated NO_2 slightly, with the NMB decreasing from -29.1% to -26.7%.

With inclusion of the soil HONO emission under the typical fertilizer use, the simulated daytime average O_3 levels increased from 68.3 to 74.5 ppb, closer to the observed average at Wangdu (74.6 ppb) (Figure 4c). The maximum increase in the hourly O_3 level was above 9 ppb. The increased oxidation capacity enhanced secondary aerosol production. The simulated nitrate concentration increased by 49% (Figure 4d) due to an increase in the oxidation of NO_x by OH and O_3 to form nitric acid. The model was able to capture the high nitrate concentrations, e.g., at night on 29 and 30 June. Here we only examined nitrate because our model had been previously improved for nitrate production processes [44], whereas the chemical processes for other secondary aerosols (e.g., sulfate, organics) are less certain in current chemical transport models [64, 65].

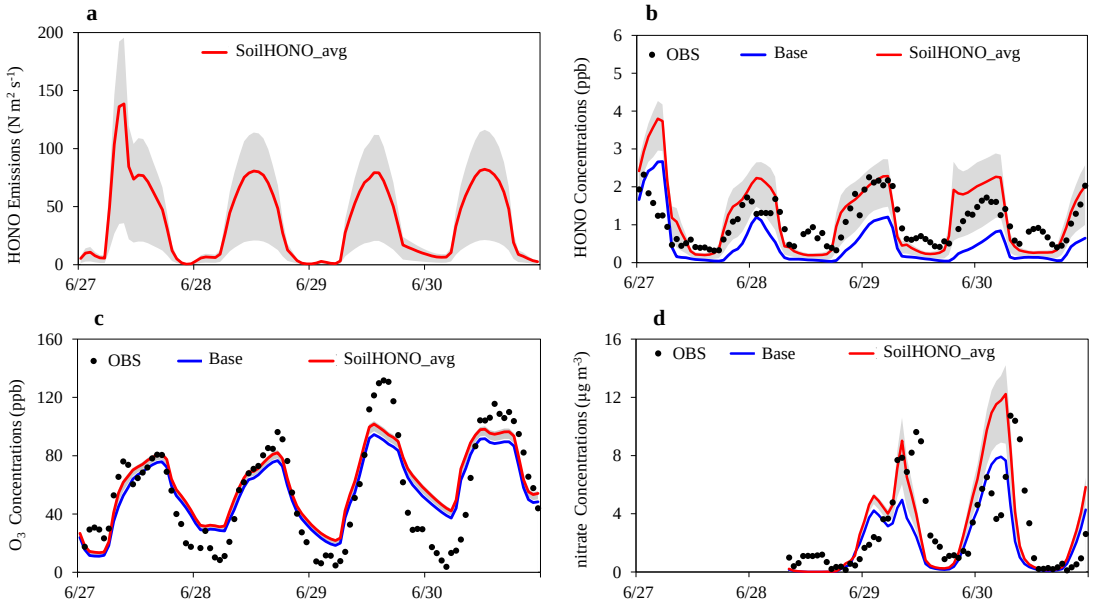

383

384 **Figure 4.** Impacts of soil HONO emissions after urea application at Wangdu in the
385 North China Plain. (a) Soil HONO emissions (F_{emis}) and the impacts on (b) HONO
386 mixing ratios, (c) O_3 mixing ratios, and (d) nitrate concentrations at the Wangdu site.
387 Nitrate observation data were not available before 8:00 on 28 June 2014 due to
388 instrument failure. The grey areas represent the range between the lowest
389 (SoilHONO_min) and highest (SoilHONO_max) HONO emission with respect to
390 SWC.

391 Figure 5 shows the potential impacts of soil HONO emissions in the NCP region for
392 the average case (SoilHONO_avg), which suggests that soil HONO emissions could
393 increase the daily ambient average HONO mixing ratio by 0.6 ppb (117%), the daytime
394 average OH concentration by 41% and O_3 by 8%. The regional daily average nitrate
395 concentration was enhanced by 47%. The absolute enhancement was more significant
396 in the areas with higher aerosol concentrations. The largest increase of nitrate exceeded

12 μg/m^3 for the simulation period average. If all of the agricultural soil reaches the wet peak of the HONO emissions (SoilHONO_max), the enhancement could be much larger and could be 0.9 ppb (164%) for the daily average HONO, 4.5 × 10^6 molecules cm^{-3} (54%) for the daytime average OH, 7.5 ppb (11%) for the daytime average O_3, and 4.2 μg m^{-3} (66%) for the daily average nitrate in the NCP region (Figure S6). The results demonstrate that crop fertilization can significantly increase HONO emission and aggravate regional air quality in the NCP. Although our model simulation is for a relatively short 4-day period, the impact of fertilization is expected to occur in extended periods in summer. In the NCP region, the main summer crop is maize, which is planted in June after harvesting wheat. Fertilizers are applied at the time of planting as basal dressing, with additional top dressing in August [63]. For a large agricultural region like NCP, the regional fertilization may last for several weeks due to different fertilization time by individual farmers. Consequently, the effects of fertilization may play a key role in atmospheric chemistry and air quality during photochemical active summer season in the NCP.

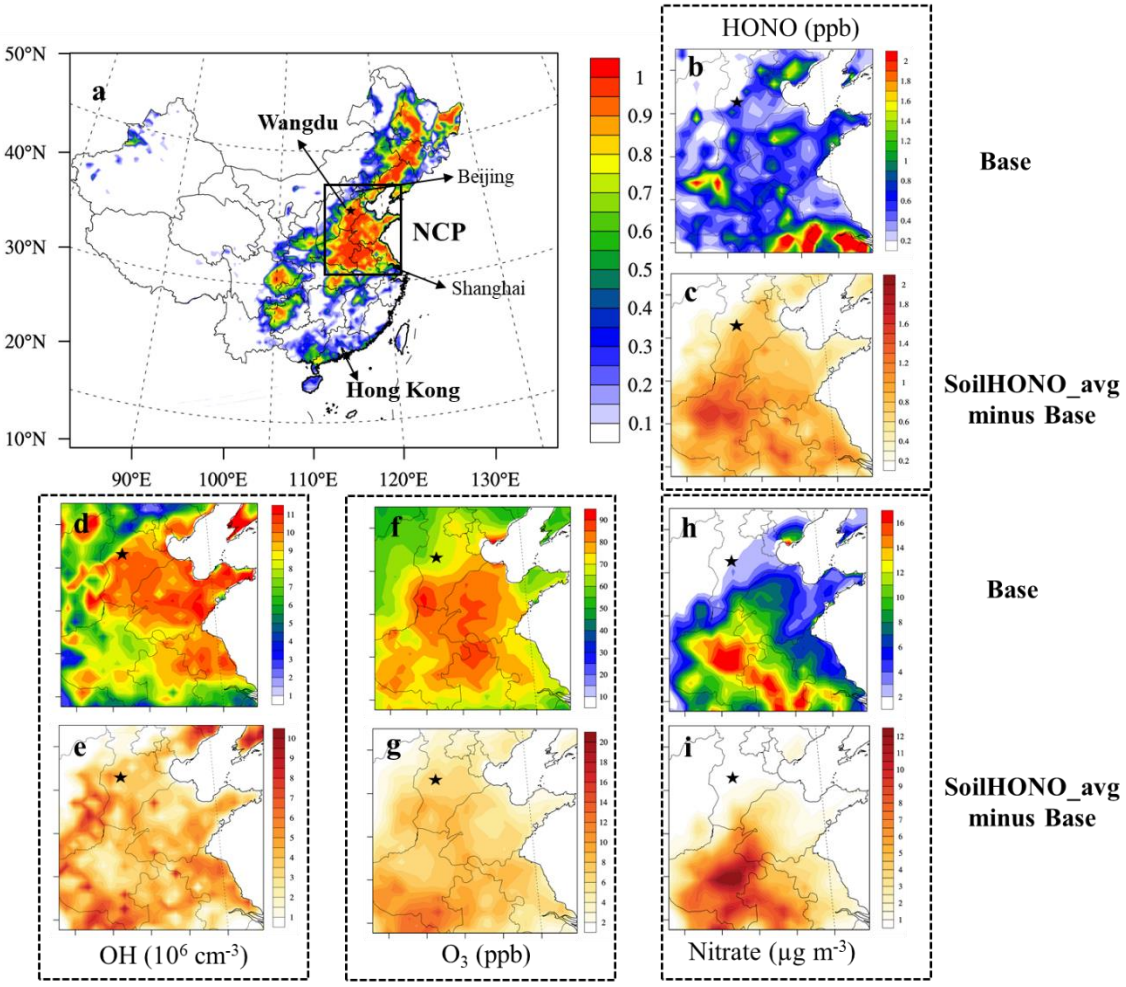

412

413 **Figure 5.** Model simulated impacts of soil HONO emissions after urea application in

414 the North China Plain. a is the distribution of cropland (unit: fraction) in China and

415 model domain. b-i are the spatial distributions of the (b, c) daily average HONO, (d, e)

416 daytime average OH, (f, g) daytime average O_3 and (h, i) daily average nitrate in the

417 Base case and the differences with SoilHONO_avg during 27–30 June 2014. The black

418 stars represent the locations of the sampling sites in Wangdu.

419 It should be noted the above simulations of regional soil HONO impact may subject

420 to uncertainty due to lack of information on fertilizer use in different croplands in the

421 simulation period and limited soil samples whose emissions were tested in our study.

Nonetheless, the soil parameterization scheme from our study enables emission-based air quality models to estimate the soil HONO emission and atmospheric impact after fertilization. Further studies are needed to quantify the soil HONO emissions from other agricultural lands and to develop a data base on gridded distribution of different fertilizer use in major agricultural regions.

IMPLICATIONS

Our study demonstrates that fertilization of soils by three widely nitrogen-based fertilizers could have important contribution to ambient HONO and in turn aggravate air pollution in the agriculture intensive NCP region of China. As the most consumed chemical fertilizer type, nitrogen fertilizers have been extensively used in the world. According to the International Fertilizer Association (IFA) [66] and China Statistical Yearbook [67], China is the world's largest N fertilizers consumer, followed by India, the USA, western and central Europe, Brazil, and Russia (Figure S9). From year 2000 to 2017, nitrogen fertilizer consumption increased by 3%-114% in these countries and 18 % in the world [66]. And the global demand is projected to increase at a rate of 1.2%/year from 2017 to 2022 and will reach 112 Tg N yr^{-1} in 2022 [1]. The potential high HONO emissions from fertilized soil and its impacts on air quality thus require worldwide attention.

Urea accounts for more than 60% of the global consumed N fertilizer [66]. In China, urea consumption has increased by approximately 49%, and its proportion in total fertilizer use increased from 63.6% in 2000 to 92.1% in 2017 (Figure 6a). In India, urea

accounts for ~99% of the total N fertilizer consumption (Figure 6b). In comparison, the USA, Europe, and Russia use more ammonium nitrate and other N fertilizers (e.g., calcium ammonium nitrate, liquid ammonia, nitrogen solutions), with urea accounting for 5%–30%. Although urea has several advantages over other nitrogen fertilizers such as its higher nitrogen content and a longer residence in soil for absorption by plants, the same properties unfortunately lead to higher emission of HONO to the atmosphere. Thus, for China and India, two countries with the highest urea use and severe air pollution, adding nitrification inhibitors [68] along urea or replacing urea with low HONO emitting fertilizers would help alleviate air pollution during the fertilization periods. We also call for investigations of the HONO emissions potential from other nitrogen fertilizers, in addition to the three studied in this work, and their environmental impacts.

ASSOCIATED CONTENT

Supporting Information

The Supporting Information is available free of charge on the ACS Publications website.

One additional Table (Table S1) and nine figures (Figures S1−S9). Parameterized HONO Source mechanisms included in the model (Table S1); schematic diagram of the dynamic chamber system (Figures S1); soil NO emission before and after fertilization (Figures S2); measured [HONO]* for Wangdu and Hong Kong samples

(Figures S3); impact of soil temperature on soil HONO emissions in Hong Kong (Figures S4); Gaussian fitting results of the soil HONO emission (Figures S5); comparison of simulated and observed meteorological factors at Wangdu site; comparison of simulated and observed NO_2 concentrations at Wangdu site (Figures S7); model simulated impacts of soil HONO emissions after urea application in the North China Plain (Figures S8); consumptions of different N fertilizers in six regions with large areas of cultivated land in 2000-2017(Figures S9).

AUTHOR INFORMATION

Corresponding Author

Tao Wang − Department of Civil and Environmental Engineering, Hong Kong Polytechnic University, Hong Kong 99907, China

ORCID: 0000-0002-4765-9377

Phone: +00852-27666059

Email: tao.wang@polyu.edu.hk

Present Addresses

‡ (X.F.) Now at Institute of Environment and Ecology, Tsinghua Shenzhen International Graduate School, Tsinghua University, 518055 Shenzhen, China

Author contributions

T.W. initiated this research. Y.W., X.F. and T.W. designed the research. Y.W. performed the lab experiment. X.F. performed the model simulations. D.W. and M.W. contributed to the chamber design. K.L. and Y.Z. contributed the field observed HONO, O_3, and NO_3^- data at Wangdu. Y.M. and Z.L. collected the soil samples at Wangdu. T.W., Y.W., X.F., and D.W. analyzed data and wrote the paper. All authors contributed to the editing and revisions of the paper.

† These authors contributed equally to this work.

Notes

The authors declare no competing financial interest.

ACKNOWLEDGMENT

This research was supported by The Hong Kong Research Grants Council (T24-504/17-N).

REFERENCES

1. FAO (Food and Agriculture Organization), World fertilizer trends and outlook to 2022. *Available at http://www.fao.org/3/ca6746en/CA6746EN.pdf?eloutlink=imf2fao (accessed 28th Aug 2021)* **2019**.

2. Mulvaney, R. L.; Khan, S. A.; Ellsworth, T. R., Synthetic nitrogen fertilizers deplete soil nitrogen: a global dilemma for sustainable cereal production. *Journal of Environmental Quality* **2009,** *38* (6), 2295-314.

3. Lu, C.; Tian, H., Global nitrogen and phosphorus fertilizer use for agriculture production in the past half century: Shifted hot spots and nutrient imbalance. *Earth System Science Data* **2017,** *9* (1), 181-192.

4. FAOSTAT (Food and Agriculture Organization Corporate Statistical Database), FAO online database. *Available at http://faostat3.fao.org/browse/G1/*/E (accessed 24th Jun 2020)* **2019**.

5. Zhang, X.; Davidson, E. A.; Mauzerall, D. L.; Searchinger, T. D.; Dumas, P.; Shen, Y., Managing nitrogen for sustainable development. *Nature* **2015,** *528* (7580), 51.

6. Mueller, N. D.; Lassaletta, L.; Runck, B. C.; Billen, G.; Garnier, J.; Gerber, J. S., Declining spatial efficiency of global cropland nitrogen allocation. *Global Biogeochemical Cycles* **2017,** *31* (2), 245-257.

7. Gheysari, M.; Mirlatifi, S. M.; Homaee, M.; Asadi, M. E.; Hoogenboom, G., Nitrate leaching in a silage maize field under different irrigation and nitrogen fertilizer rates. *Agricultural Water Management* **2009,** *96* (6), 946.

8. Sepaskhah, A. R.; Tafteh, A., Yield and nitrogen leaching in rapeseed field under different nitrogen rates and water saving irrigation. *Agricultural Water Management* **2012,** *112*, 55-62.

9. Tafteh, A.; Sepaskhah, A. R., Application of HYDRUS-1D model for simulating water and nitrate leaching from continuous and alternate furrow irrigated rapeseed and maize fields. *Agricultural Water Management* **2012,** *113*, 19-29.

10. Ju, X.; Zhang, C., Nitrogen cycling and environmental impacts in upland agricultural soils in North China: A review. *Journal of Integrative Agriculture* **2017,** *16* (12), 2848-2862.

11. Bouwman, A. F.; Boumans, L. J. M.; Batjes, N. H., Emissions of N_2O and NO from fertilized fields: Summary of available measurement data. *Global Biogeochemical Cycles* **2002,** *16* (4), 6-1-6-13.

12. Zhu, X.; Burger, M.; Doane, T. A.; Horwath, W. R., Ammonia oxidation pathways and nitrifier denitrification are significant sources of N_2O and NO under low oxygen availability. *Proceedings of the National Academy of Sciences of the United States of America* **2013,** *110* (16), 6328-33.

13. Oswald, R.; Behrendt, T.; Ermel, M.; Wu, D.; Su, H.; Cheng, Y.; Breuninger, C.; Moravek, A.; Mougin, E.; Delon, C., HONO emissions from soil bacteria as a major source of atmospheric reactive nitrogen. *Science* **2013,** *341* (6151), 3.

14. Wu, D.; Horn, M. A.; Behrendt, T.; Muller, S.; Li, J.; Cole, J. A.; Xie, B.; Ju, X.; Li, G.; Ermel, M.; Oswald, R.; Frohlich-Nowoisky, J.; Hoor, P.; Hu, C.; Liu, M.; Andreae, M. O.; Poschl, U.; Cheng, Y.; Su, H.; Trebs, I.; Weber, B.; Sorgel,

538 M., Soil HONO emissions at high moisture content are driven by microbial nitrate
539 reduction to nitrite: tackling the HONO puzzle. *The ISME Journal* **2019,** *13* (7), 1688-
540 1699.

541 15. Alicke, B.; Geyer, A.; Hofzumahaus, A.; Holland, F.; Konrad, S.; Patz, H.
542 W.; Schafer, J.; Stutz, J.; Volz-Thomas, A.; Platt, U., OH formation by HONO
543 photolysis during the BERLIOZ experiment. *Journal of Geophysical Research* **2003,**
544 *108* (D4).

545 16. Kim, S.; Vandenboer, T. C.; Young, C. J.; Riedel, T. P.; Thornton, J. A.;
546 Swarthout, B.; Sive, B.; Lerner, B.; Gilman, J.; Warneke, C., The primary and
547 recycling sources of OH during the NACHTT-2011 campaign: HONO as an important
548 OH primary source in the wintertime. *Journal of Geophysical Research* **2014,** *119*,
549 6886-6896.

550 17. Tan, Z.; Fuchs, H.; Lu, K.; Hofzumahaus, A.; Bohn, B.; Broch, S.; Dong,
551 H.; Gomm, S.; H?Seler, R.; He, L., Radical chemistry at a rural site (Wangdu) in the
552 North China Plain: observation and model calculations of OH, HO_2 and RO_2 radicals.
553 *Atmospheric Chemistry and Physics* **2017,** *17* (1), 663-690.

554 18. Fu, X.; Wang, T.; Zhang, L.; Li, Q.; Wang, Z., The significant contribution
555 of HONO to secondary pollutants during a severe winter pollution event in southern
556 China. *Atmospheric Chemistry Physics* **2019,** *19* (1), 1-14.

19. Michoud, V.; Colomb, A.; Borbon, A.; Miet, K.; Beekmann, M.; Camredon, M.; Aumont, B.; Perrier, S.; Zapf, P.; Siour, G.; Ait-Helal, W.; Afif, C.; Kukui, A.; Furger, M.; Dupont, J. C.; Haeffelin, M.; Doussin, J. F., Study of the unknown HONO daytime source at a European suburban site during the MEGAPOLI summer and winter field campaigns. *Atmospheric Chemistry and Physics* **2014,** *14* (6), 2805-2822.

20. Zhang, W.; Tong, S.; Jia, C.; Wang, L.; Liu, B.; Tang, G.; Ji, D.; Hu, B.; Liu, Z.; Li, W.; Wang, Z.; Liu, Y.; Wang, Y.; Ge, M., Different HONO Sources for Three Layers at the Urban Area of Beijing. *Environ Sci Technol* **2020,** *54* (20), 12870-12880.

21. Ermel, M.; Behrendt, T.; Oswald, R.; Derstroff, B.; Wu, D.; Hohlmann, S.; Stönner, C.; Pommerening-Röser, A.; Könneke, M.; Williams, J.; Meixner, F. X.; Andreae, M. O.; Trebs, I.; Sörgel, M., Hydroxylamine released by nitrifying microorganisms is a precursor for HONO emission from drying soils. *Scientific Reports* **2018,** *8* (1), 1877.

22. Butterbach-Bahl, K.; Baggs, E. M.; Dannenmann, M.; Kiese, R.; Zechmeister-Boltenstern, S., Nitrous oxide emissions from soils: how well do we understand the processes and their controls? *Philos Trans R Soc Lond B Biol Sci* **2013,** *368* (1621), 20130122.

575 23. Ludwig, J.; Meixner, F. X.; Vogel, B.; Forstner, J., Soil-air exchange of nitric
576 oxide: An overview of processes, environmental factors, and modeling studies.
577 *Biogeochemistry* **2001,** *52*, 33.

578 24. Bollmann, A.; Conrad, R., Influence of O_2 availability on NO and N_2O release
579 by nitrification and denitrification in soils. *Global Change Biology* **1998,** *4*, 387-396.

580 25. Tang, K.; Qin, M.; Duan, J.; Fang, W.; Meng, F.; Liang, S.; Xie, P.; Liu,
581 J.; Liu, W.; Xue, C.; Mu, Y., A dual dynamic chamber system based on IBBCEAS for
582 measuring fluxes of nitrous acid in agricultural fields in the North China Plain.
583 *Atmospheric Environment* **2019,** *196*, 10-19.

584 26. Xue, C.; Ye, C.; Zhang, Y.; Ma, Z.; Liu, P.; Zhang, C.; Zhao, X.; Liu, J.;
585 Mu, Y., Development and application of a twin open-top chambers method to measure
586 soil HONO emission in the North China Plain. *Science of the Total Environment* **2019,**
587 *659*, 621-631.

588 27. Liu, Y.; Lu, K.; Li, X.; Dong, H.; Tan, Z.; Wang, H.; Zou, Q.; Wu, Y.;
589 Zeng, L.; Hu, M.; Min, K. E.; Kecorius, S.; Wiedensohler, A.; Zhang, Y., A
590 comprehensive model test of the HONO sources constrained to field measurements at
591 rural North China Plain. *Environmental Science & Technology* **2019,** *53* (7), 3517-3525.

592 28. Xue, C.; Ye, C.; Zhang, C.; Catoire, V.; Liu, P.; Gu, R.; Zhang, J.; Ma, Z.;
593 Zhao, X.; Zhang, W.; Ren, Y.; Krysztofiak, G.; Tong, S.; Xue, L.; An, J.; Ge, M.;
594 Mellouki, A.; Mu, Y., Evidence for Strong HONO Emission from Fertilized

595 Agricultural Fields and its Remarkable Impact on Regional O_3 Pollution in the Summer
596 North China Plain. *ACS Earth and Space Chemistry* **2021,** *5* (2), 340-347.

597 29. Gao, J.; Xie, Y.; Jin, H.; Liu, Y.; Bai, X.; Ma, D.; Zhu, Y.; Wang, C.; Guo,
598 T., Nitrous oxide emission and denitrifier abundance in two agricultural soils amended
599 with crop residues and urea in the north china plain. *PLoS One* **2016,** *11* (5), e0154773.

600 30. Su, H.; Cheng, Y.; Oswald, R.; Behrendt, T.; Trebs, I.; Meixner, F. X.;
601 Andreae, M.; Cheng, P.; Zhang, Y., Soil nitrite as a source of atmospheric HONO and
602 OH radicals. *Science* **2011,** *333* (6049), p.1616-1618.

603 31. Ma, F.; Gao, H.; Eneji, A. E.; Jin, Z.; Han, L.; Liu, J., An economic valuation
604 of groundwater management for agriculture in Luancheng county, North China.
605 *Agricultural Water Management* **2016,** *163*, 28-36.

606 32. Wang, J.; Wang, E.; Yang, X.; Zhang, F.; Yin, H., Increased yield potential
607 of wheat-maize cropping system in the North China Plain by climate change adaptation.
608 *Climatic Change* **2012,** *113* (3-4), 825-840.

609 33. Wong, S. C.; Li, X. D.; Zhang, G.; Qi, S. H.; Min, Y. S., Heavy metals in
610 agricultural soils of the Pearl River Delta, South China *Environmental Pollution* **2001,**
611 *119*, 33-44.

612 34. Behrendt, T.; Braker, G.; Song, G.; Pommerenke, B.; Dörsch, P., Nitric oxide
613 emission response to soil moisture is linked to transcriptional activity of functional
614 microbial groups. *Soil Biology and Biochemistry* **2017,** *115*, 337-345.

615 35. Behrendt, T.; Veres, P. R.; Ashuri, F.; Song, G.; Flanz, M.; Mamtimin, B.;
616 Bruse, M.; Williams, J.; Meixner, F. X., Characterisation of NO production and
617 consumption: new insights by an improved laboratory dynamic chamber technique.
618 *Biogeosciences* **2014,** *11* (19), 5463-5492.

619 36. Bhadha, J. H.; Capasso, J. M.; Khatiwada, R.; Swanson, S.; LaBorde, C.,
620 Raising soil organic matter content to Improve water holding capacity. *UF/IFAS*
621 *Extension* **2017,** *SL447*.

622 37. Ye, C.; Gao, H.; Zhang, N.; Zhou, X., Photolysis of nitric acid and nitrate on
623 natural and artificial Surfaces. *Environmental Science & Technology* **2016,** *50* (7),
624 3530-6.

625 38. Ye, C.; Zhang, N.; Gao, H.; Zhou, X., Photolysis of particulate nitrate as a
626 source of HONO and NOx. *Environmental Science & Technology* **2017,** *51* (12), 6849-
627 6856.

628 39. VandenBoer, T. C.; Young, C. J.; Talukdar, R. K.; Markovic, M. Z.; Brown,
629 S. S.; Roberts, J. M.; Murphy, J. G., Nocturnal loss and daytime source of nitrous acid
630 through reactive uptake and displacement. *Nature Geoscience* **2014,** *8* (1), 55-60.

631 40. van Dijk, S. M.; Gut, A.; Kirkman, G. A.; Meixner, F. X.; Andreae, M. O.,
632 Biogenic NO emissions from forest and pasture soils: Relating laboratory studies to
633 field measurements. *Journal of Geophysical Research* **2002,** *107* (D20).

634 41. Mamtimin, B.; Meixner, F. X.; Behrendt, T.; Badawy, M.; Wagner, T., The
635 contribution of soil biogenic NO and HONO emissions from a managed hyperarid
636 ecosystem to the regional NOx emissions during growing season. *Atmospheric*
637 *Chemistry and Physics* **2016,** *16* (15), 10175-10194.

638 42. Meusel, H.; Tamm, A.; Kuhn, U.; Wu, D.; Leifke, A. L.; Fiedler, S.;
639 Ruckteschler, N.; Yordanova, P.; Lang-Yona, N.; Pöhlker, M.; Lelieveld, J.;
640 Hoffmann, T.; Pöschl, U.; Su, H.; Weber, B.; Cheng, Y., Emission of nitrous acid
641 from soil and biological soil crusts represents an important source of HONO in the
642 remote atmosphere in Cyprus. *Atmospheric Chemistry and Physics* **2018,** *18* (2), 799-
643 813.

644 43. Pan, H. X.; Zhu, G. F.; ZHang, Y.; Guo, H. W.; Yong, L. L.; Wan, Q. Z.;
645 Ma, H. Y.; Li, S., Spatial and temporal variations of relative soil moisture in China's
646 farmland (in Chinese). *Acta Geographica Sinica* **2019,** *74* (1), 13.

647 44. Fu, X.; Wang, T.; Gao, J.; Wang, P.; Liu, Y.; Wang, S.; Zhao, B.; Xue, L.,
648 Persistent heavy winter nitrate pollution driven by increased photochemical oxidants in
649 Northern China. *Environmental Science & Technology* **2020,** *54* (7), 3881-3889.

650 45. Tang, G.; Zhang, J.; Zhu, X.; Song, T.; Münkel, C.; Hu, B.; Schäfer, K.;
651 Liu, Z.; Zhang, J.; Wang, L.; Xin, J.; Suppan, P.; Wang, Y., Mixing layer height and
652 its implications for air pollution over Beijing, China. *Atmospheric Chemistry and*
653 *Physics* **2016,** *16* (4), 2459-2475.

654 46. Pan, L.; Xu, J.; Tie, X.; Mao, X.; Gao, W.; Chang, L., Long-term
655 measurements of planetary boundary layer height and interactions with $PM_{2.5}$ in
656 Shanghai, China. *Atmospheric Pollution Research* **2019,** *10* (3), 989-996.

657 47. Zhao, B.; Zheng, H.; Wang, S.; Smith, K. R.; Lu, X.; Aunan, K.; Gu, Y.;
658 Wang, Y.; Ding, D.; Xing, J.; Fu, X.; Yang, X.; Liou, K. N.; Hao, J., Change in
659 household fuels dominates the decrease in $PM_{2.5}$ exposure and premature mortality in
660 China in 2005-2015. *Proceedings of the National Academy of Sciences of the United*
661 *States of America* **2018,** *115* (49), 12401-12406.

662 48. Guenther, A.; Karl, T.; Harley, P.; Wiedinmyer, C.; Palmer, P. I.; Geron, C.,
663 Estimates of global terrestrial isoprene emissions using MEGAN (Model of Emissions
664 of Gases and Aerosols from Nature). *Atmospheric Chemistry and Physics* **2006,** *6* (11),
665 3181-3210.

666 49. Cartes, P.; Jara, A. A.; Demanet, R.; María, L. M., Urease activity and
667 nitrogen mineralization kinetics as affected by temperature and urea input rate in
668 southern Chilean Andisols. *Journal of Soil Science and Plant Nutrition* **2009,** *9* (1), 14.

669 50. Bouwman, A. F.; Lee, D. S.; Asman, W. A. H.; Dentener, F. J.; Van Der
670 Hoek, K. W.; Olivier, J. G. J., A global high-resolution emission inventory for ammonia.
671 *Global Biogeochemical Cycles* **1997,** *11* (4), 561-587.

672 51. Ouyang, Y.; Evans, S. E.; Friesen, M. L.; Tiemann, L. K., Effect of nitrogen
673 fertilization on the abundance of nitrogen cycling genes in agricultural soils: A meta-
674 analysis of field studies. *Soil Biology and Biochemistry* **2018,** *127*, 71-78.

675 52. Jin, Z. J.; Li, L. Q.; Liu, X. Y.; Pan, G. X.; Qaiser, H.; Liu, Y. Z., Impact of
676 long-term fertilization on community structure of ammonia oxidizing and denitrifying
677 bacteria based on amoA and nirK Genes in a rice paddy from Tai Lake region, China.
678 *Journal of Integrative Agriculture* **2014,** *13* (10), 2286-2298.

679 53. Di, H. J.; Cameron, K. C.; Podolyan, A.; Robinson, A., Effect of soil moisture
680 status and a nitrification inhibitor, dicyandiamide, on ammonia oxidizer and denitrifier
681 growth and nitrous oxide emissions in a grassland soil. *Soil Biology and Biochemistry*
682 **2014,** *73*, 59-68.

683 54. Shen, L. D.; Liu, S.; Lou, L. P.; Liu, W. P.; Xu, X. Y.; Zheng, P.; Hu, B.
684 L., Broad distribution of diverse anaerobic ammonium-oxidizing bacteria in chinese
685 agricultural soils. *Appl Environ Microbiol* **2013,** *79* (19), 6167-72.

686 55. Wrage, N.; Velthof, M. L.; Beusichem, v.; Oenema, O., Role of nitrifier
687 denitrification in the production of nitrous oxide. *Soil Biology and Biochemistry* **2001,**
688 *33*, 1723-1732.

689 56. Carrasco, D.; Fernandez-Valiente, E.; Ariosa, Y.; Quesada, A., Measurement
690 of coupled nitrification-denitrification in paddy fields affected by Terrazole, a
691 nitrification inhibitor. *Biology and Fertility of Soils* **2004,** *39* (3), 186-192.

692 57. Zhou, S.; Sakiyama, Y.; Riya, S.; Song, X.; Terada, A.; Hosomi, M.,
693 Assessing nitrification and denitrification in a paddy soil with different water dynamics
694 and applied liquid cattle waste using the ^{15}N isotopic technique. *Science of the Total*
695 *Environment* **2012,** *430*, 93-100.

696 58. Bolan, N. S.; Saggar, S.; Luo, J. F.; Bhandral, R.; Singh, J., Gaseous
697 emissions of nitrogen from grazed pastures: processes, measurements and modelling,
698 environmental implications, and mitigation. *Advances in Agronomy* **2004,** *84*, 288-295.

699 59. Rodriguez, M. J.; Saggar, S.; Berben, P.; Palmada, T.; Lopez-Villalobos, N.;
700 Pal, P., Use of a urease inhibitor to mitigate ammonia emissions from urine patches.
701 *Environmental Technology* **2019**, 1-12.

702 60. Liu, R.; He, J.; Zhang, L., Response of nitrification/denitrification and their
703 associated microbes to soil moisture change in paddy soil (in Chinese). *Environmental*
704 *Science* **2014,** *35*, 4275-4283.

705 61. Mulvaney, R. L.; Khan, S. A.; Mulvaney, C. S., Nitrogen fertilizers promote
706 denitrification. *Biology and Fertility of Soils* **1997,** *24* (2), 211-220.

62. Venterea, R. T., Nitrite-driven nitrous oxide production under aerobic soil conditions: kinetics and biochemical controls. *Global Change Biology* **2007,** *13* (8), 1798-1809.

63. Zhang, Y.; Mu, Y.; Zhou, Y.; Liu, J.; Zhang, C., Nitrous oxide emissions from maize–wheat field during 4 successive years in the North China Plain. *Biogeosciences* **2014,** *11* (7), 1717-1726.

64. Zhao, B.; Wang, S.; Donahue, N. M.; Jathar, S. H.; Huang, X.; Wu, W.; Hao, J.; Robinson, A. L., Quantifying the effect of organic aerosol aging and intermediate-volatility emissions on regional-scale aerosol pollution in China. *Scientific Reports* **2016,** *6*, 28815.

65. Wang, Y.; Zhang, Q.; Jiang, J.; Zhou, W.; Wang, B.; He, K.; Duan, F.; Zhang, Q.; Philip, S.; Xie, Y., Enhanced sulfate formation during China's severe winter haze episode in January 2013 missing from current models. *Journal of Geophysical Research: Atmospheres* **2014,** *119* (17), 10,425-10,440.

66. IFA (International Fertilizer Association), World nitrogen fertilizer consumption. *Available at http://www.fertilizer.org (accessed 9th Aug 2020)* **2000-2017**.

67. National Bureau of Statistics, China Statistical Yearbooks. *Statistical Press: Beijing* **2019**.

725 68. Woodward, E. E.; Edwards, T. M.; Givens, C. E.; Kolpin, D. W.; Hladik, M.
726 L., Widespread Use of the Nitrification Inhibitor Nitrapyrin: Assessing Benefits and
727 Costs to Agriculture, Ecosystems, and Environmental Health. *Environ Sci Technol*
728 **2021,** *55* (3), 1345-1353.

729

730 **For Table of Contents Only**

731 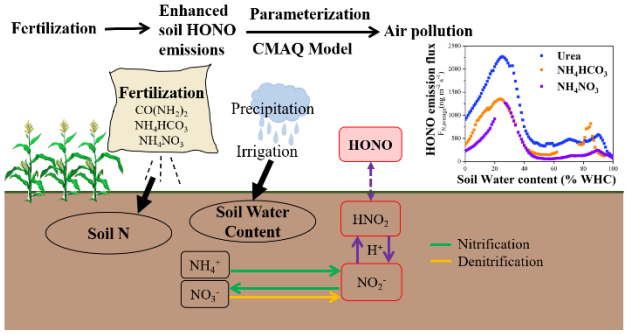

Supporting Information for

Agricultural fertilization aggravates air pollution by stimulating soil nitrous acid emissions at high soil moisture

Yanan Wang[1†], *Xiao Fu*[1,‡†], *Dianming Wu*[2], *Mengdi Wang*[2], *Keding Lu*[3], *Yujing Mu*[4,5], *Zhiguo Liu*[4,5], *Yuanhang Zhang*[3], *Tao Wang*[1*]

[1] Department of Civil and Environmental Engineering, The Hong Kong Polytechnic University, 999077 Hong Kong, China

[2] Key Laboratory of Geographic Information Sciences (Ministry of Education), School of Geographical Sciences, East China Normal University, 200241 Shanghai, China

[3] State Key Joint Laboratory of Environment Simulation and Pollution Control, College of Environmental Sciences and Engineering, Peking University, 100871 Beijing, China

[4] Research Center for Eco-Environmental Sciences, Chinese Academy of Sciences, 100085 Beijing, China

[5] University of Chinese Academy of Sciences, 100049 Beijing, China

[‡] Now at Institute of Environment and Ecology, Tsinghua Shenzhen International Graduate School, Tsinghua University, 518055 Shenzhen, China

[†] These authors contributed equally to this work.

[*] **Correspondence to:** Tao Wang

Email: cetwang@polyu.edu.hk, +00852-27666059

This PDF file includes ten pages.

The list of Table S1 and Figures S1 to S9:

Table S1. Parameterized HONO source mechanisms included in the model.

Sources	HONO formation reactions	Parameters
Vehicle emissions [1]		Gasoline: 0.8% NO_x of transportation sources; Diesel: 2.3% NO_x of transportation sources
Homogeneous reaction [1]	NO + OH→ HONO	CMAQ default
NO_2 + surface + hv + RH [1]	NO_2 + surface + hv + RH→ HONO	Nighttime: $k = 5 \times 10^{-5} \times f_{RH} \times \frac{S}{V}$ Daytime: $k = 1 \times 10^{-3} \times f_{RH} \times \frac{S}{V} \times \frac{light\ intensity}{400}$ $f_{RH} = \begin{cases} \frac{RH}{50} & (RH < 50) \\ \frac{RH}{10} - 4 & (50 \le RH \le 80) \\ 4 & (RH \ge 80) \end{cases}$
Particulate NO_3^- + hv [1, 2]	NO_3^- + hv→ HONO	$J_{PNO_3} = \frac{\frac{6.1 \times 10^{-4} \times ln(1 + 4.4 \times 10^{-1}[pNO_3])}{[pNO_3]} - 3.5 \times 10^{-5}}{7 \times 10^{-7}} \times J_{HNO_3-CMAQ}$
Deposited HNO_3/ NO_3^- + hv [1, 3]	HNO_3/NO_3^- + hv→HONO	$J_{DNO_3} = \frac{\frac{8.5 \times 10^{-4}}{2.5 \times 10^7 \times D_{NO_3}} ln(1 + 2.5 \times 10^7 D_{NO_3}) + 3.0 \times 10^{-6}}{7 \times 10^{-7}} \times J_{HNO_3-CMAQ}$

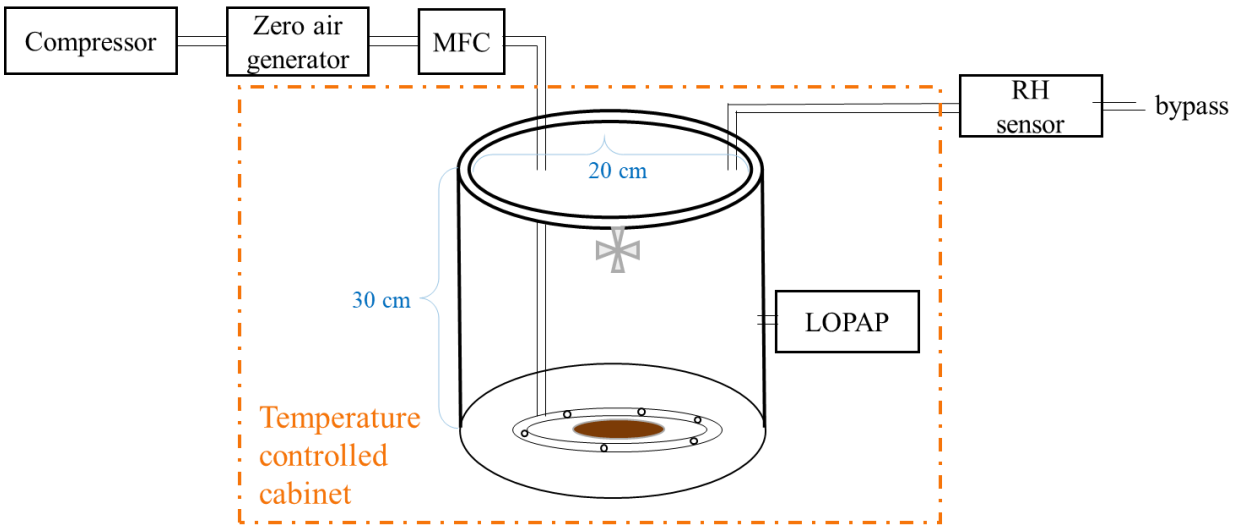

Figure S1. Schematic diagram of the dynamic chamber system.

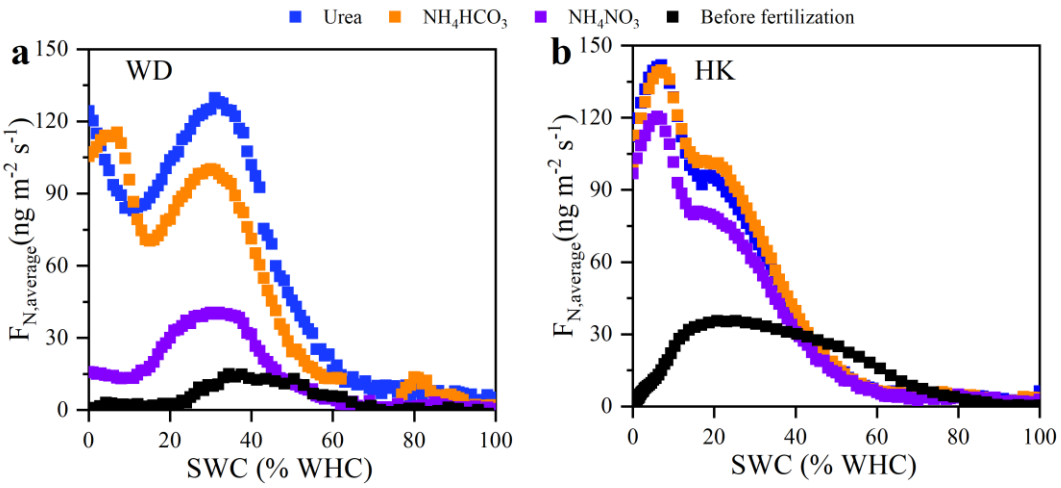

Figure S2. Soil NO emission before and after fertilization. The black squares indicate the NO emissions before fertilization for (a) S_{WD} and (b) S_{HK}. The blue, orange, purple squares represent the NO emissions after applying urea, NH_4HCO_3, and NH_4NO_3, respectively.

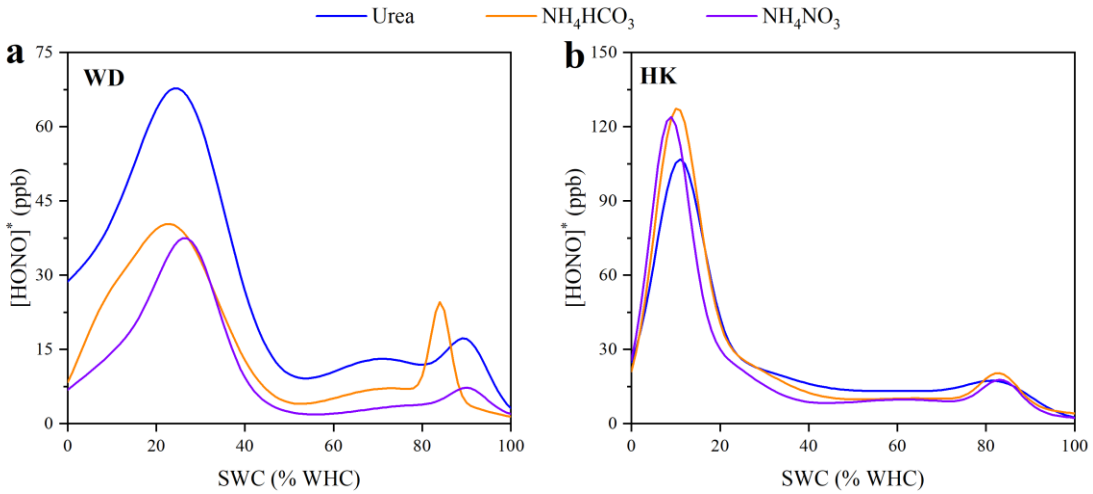

Figure S3. Measured [HONO]* for (a)Wangdu (WD) and (b) Hong Kong (HK) samples. [HONO]* is the equilibrium concentration at the soil surface [4]. Here we assumed the gas in the dynamic chamber was evenly mixed, and the measured HONO mixing ratio was used to represent [HONO]*. The [HONO]* shown here is the result obtained using multiple Gaussian fittings.

Fit1: $F_N(T) = 6.182 \cdot 10^9 \cdot \exp\left[\left(\frac{-43990}{R} \cdot \frac{1}{T}\right)\right]$ R^2=0.97

Fit2: $F_N(T) = 3.384 \cdot 10^{12} \cdot \exp\left[\left(\frac{-60642}{R} \cdot \frac{1}{T}\right)\right]$ R^2=0.98

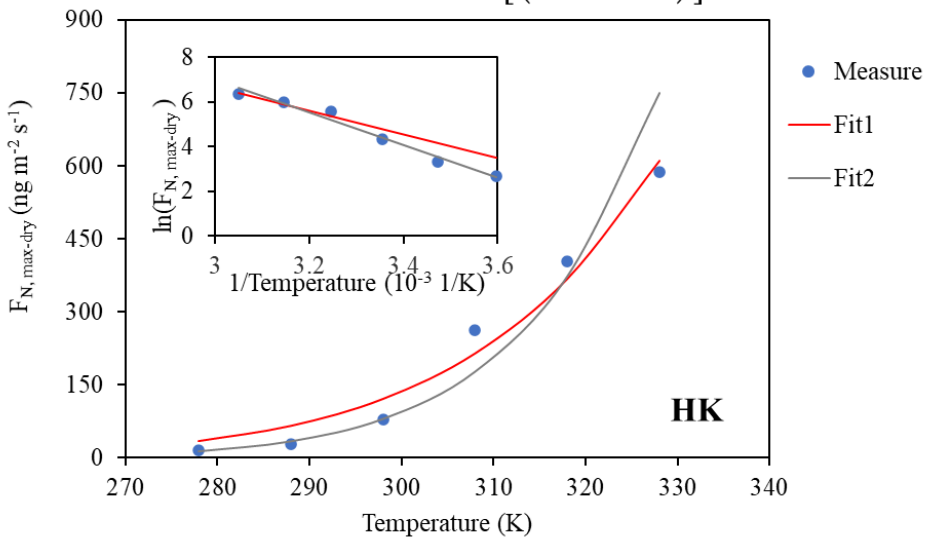

Figure S4. Impact of soil temperature on soil HONO emissions in Hong Kong. The temperature in the chamber was regulated between 5 °C and 55 °C with a step of 10 °C. The flux measurement procedure was the same as that described in Methods. The blue dot is the flux measured in the laboratory, and the red and gray lines represent two different fitting results. Fit 1 is exponential fit, and the inset in the figure is the log-transformation of the flux as the function of the inverse temperature with the red line representing the flux calculated using exponential fit parameter. Fit1 over predicts the HONO emission at temperatures below ~300 K (27 °C), but under predict it above ~310 K (37 °C). The other fitting (Fit 2) is to first log-transform the emission data and then linearly fit the data as a function of inverse temperature. We tried Fit 2, yielding $F_N(T) = 3.384 \cdot 10^{12} \cdot \exp\left[\left(\frac{-60642}{R}\right) \cdot \frac{1}{T}\right]$, which has a larger activation term compared to

the exponential Fit1 ($F_N(T)= 6.182 \cdot 10^9 \cdot \exp\left[\left(\frac{-43990}{R}\right) \cdot \frac{1}{T}\right]$). Fit 2 is better at temperature below 300 K but has under predict more at 310 K. The model simulated soil temperature at Wandu is 19 - 43 °C (292 - 316 K), with daytime temperature in the range of 25 - 43 °C (298 - 316 K). Thus, we chose the Fit1 as it may better simulate daytime HONO flux.

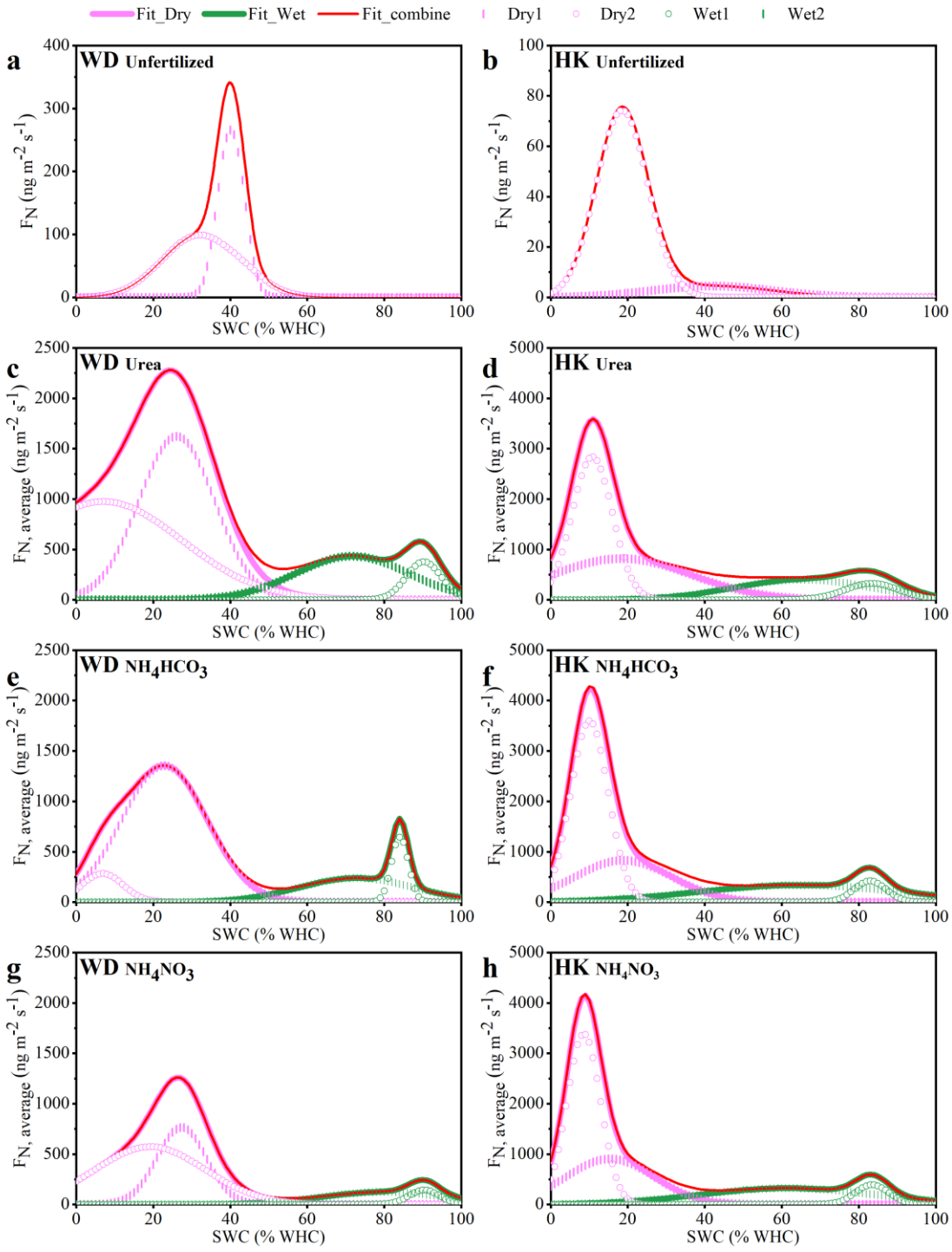

Figure S5. Gaussian fitting results of the soil HONO emission. The pink vertical lines and the pink hollow circles represent Dry1 and Dry2 at low SWC (0%–60% WHC), respectively, and the pink lines represent summation of Dry1 and Dry2 (Dry1+Dry2). The green lines (Wet1 (green hollow circles) + Wet2 (green vertical lines)) represent the fitting results at high SWC (60%–100% WHC). The red lines are the fitting curves in entire SWC range.

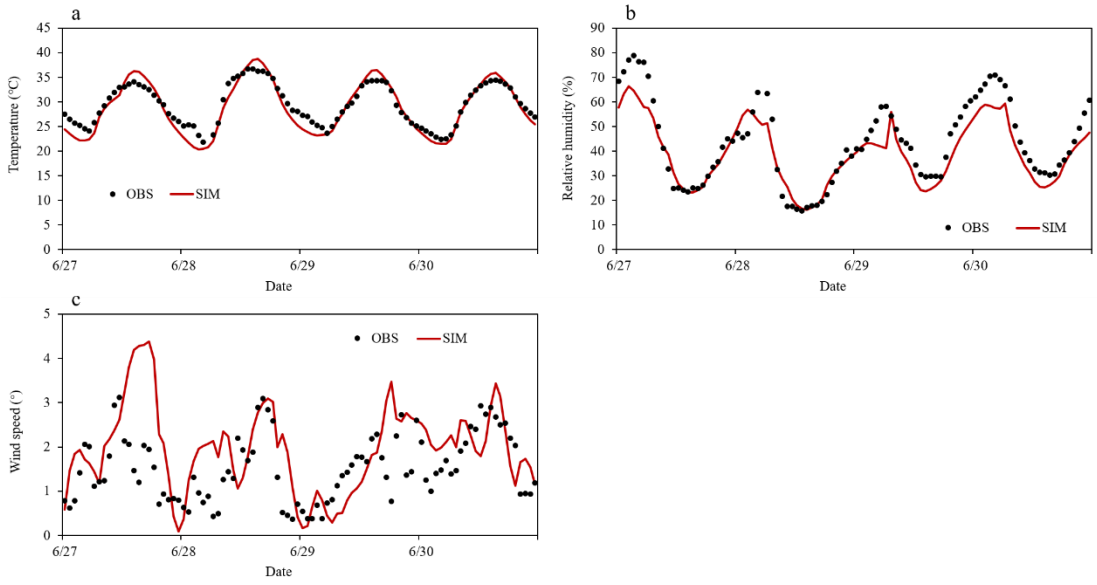

Figure S6. Comparison of simulated and observed meteorological factors at Wangdu site. (a) is temperature, (b) is relative humidity, and (c) is wind speed.

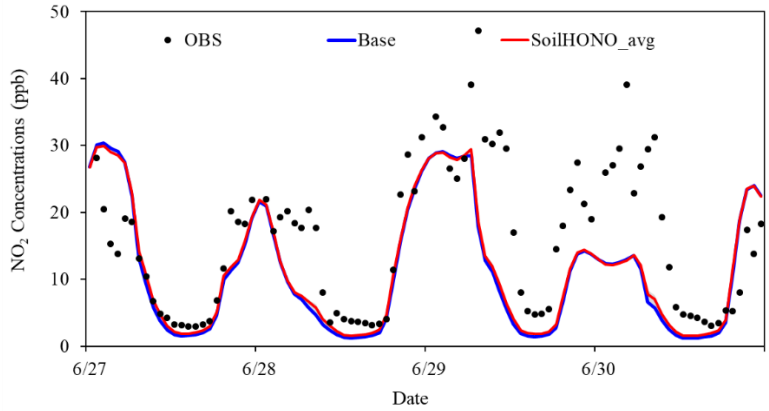

Figure S7. Comparison of simulated and observed NO_2 concentrations at Wangdu site.

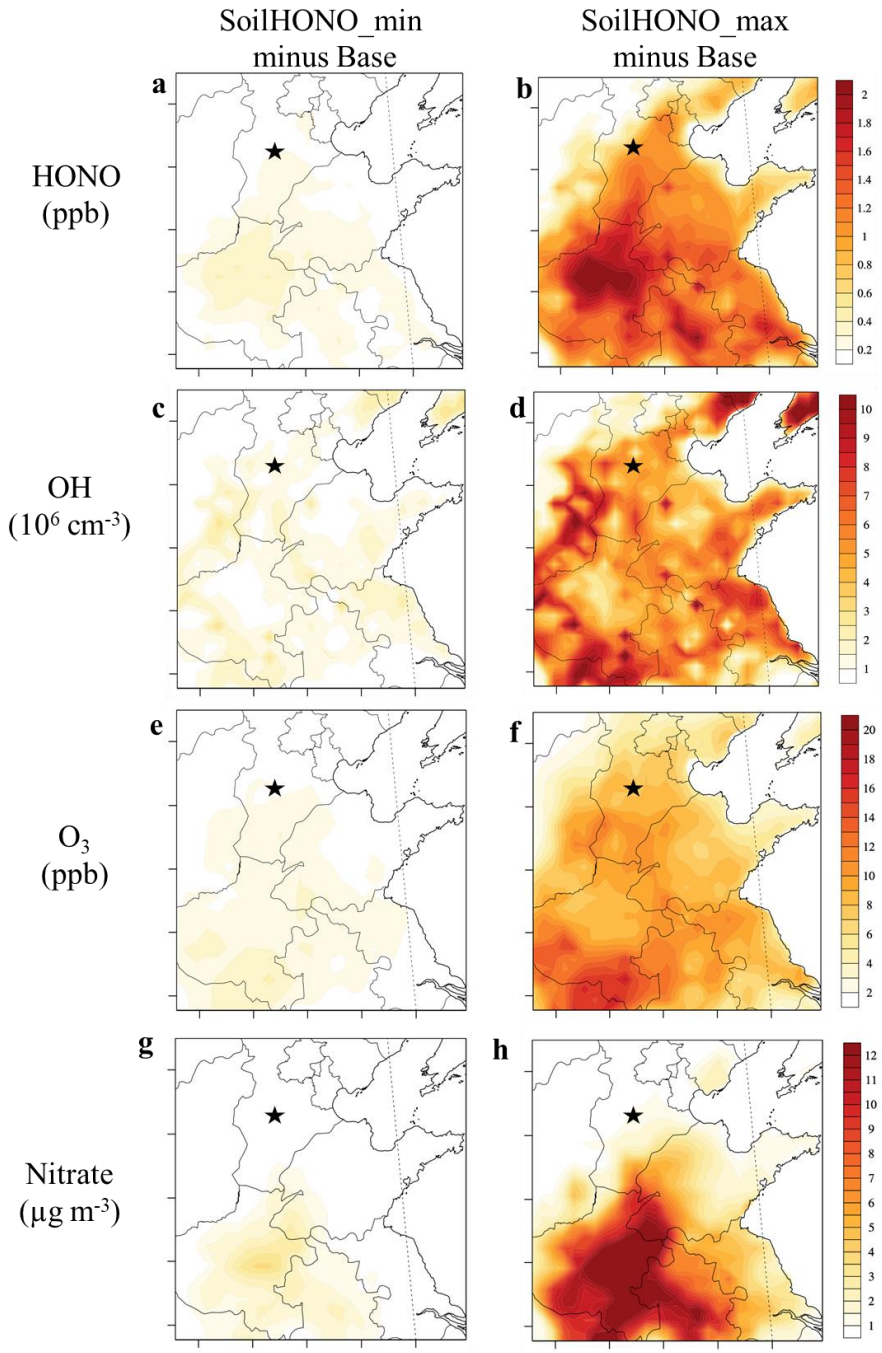

Figure S8. Model simulated impacts of soil HONO emissions after urea application in the North China Plain. The differences of Base case with SoilHONO_min and SoilHONO_max for the (a, b) daily average HONO, (c, d) daytime average OH, (e, f) daytime average O_3, and (g, h) daily average nitrate. The black stars represent the locations of the sampling sites in Wangdu.

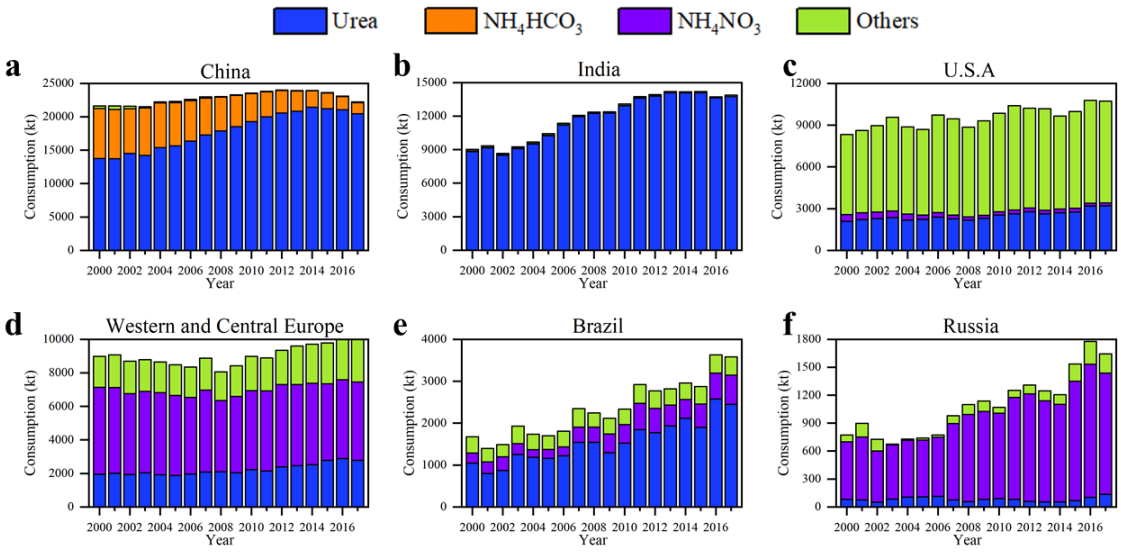

Figure S9. Consumptions of different N fertilizers in six regions with large areas of cultivated land in 2000-2017. The blue, orange, purple, and green bars represent the consumption of urea, NH_4HCO_3, NH_4NO_3 and other fertilizers, respectively.

SI References

1. Fu, X.; Wang, T.; Zhang, L.; Li, Q.; Wang, Z., The significant contribution of HONO to secondary pollutants during a severe winter pollution event in southern China. *Atmospheric Chemistry Physics* **2019,** *19* (1), 1-14.

2. Ye, C.; Zhang, N.; Gao, H.; Zhou, X., Photolysis of particulate nitrate as a source of HONO and NOx. *Environmental Science & Technology* **2017,** *51* (12), 6849-6856.

3. Ye, C.; Gao, H.; Zhang, N.; Zhou, X., Photolysis of nitric acid and nitrate on natural and artificial Surfaces. *Environmental Science & Technology* **2016,** *50* (7), 3530-6.

4. Meusel, H.; Tamm, A.; Kuhn, U.; Wu, D.; Leifke, A. L.; Fiedler, S.; Ruckteschler, N.; Yordanova, P.; Lang-Yona, N.; Pöhlker, M.; Lelieveld, J.; Hoffmann, T.; Pöschl, U.; Su, H.; Weber, B.; Cheng, Y., Emission of nitrous acid from soil and biological soil crusts represents an important source of HONO in the remote atmosphere in Cyprus. *Atmospheric Chemistry and Physics* **2018,** *18* (2), 799-813.